Available online at www.sciencedirect.com
ScienceDirect
International Journal of Solids and Structures 43 (2006) 7593–7608
INTERNATIONAL JOURNAL OF SOLIDS and STRUCTURES
www.elsevier.com/locate/ijsolstr

Analysis of quantum-dot-induced strain and electric fields in piezoelectric semiconductors of general anisotropy

C.-Y. Wang [a,*], M. Denda [b], E. Pan [c]

[a] *Mathematics and Modelling Department, Schlumberger-Doll Research, Old Quarry RD, Ridgefield, CT 06877-4108, USA*
[b] *Mechanical and Aerospace Engineering Department, Rutgers University, 98 Brett Road, Piscataway, NJ 08854-8058, USA*
[c] *Advanced Material and Structure Center, College of Engineering, University of Akron, Akron, OH 44325-3905, USA*

Received 12 January 2006; received in revised form 2 March 2006
Available online 28 March 2006

Abstract

Characteristics of the self-organized quantum dots (QDs) such as electron and hole energy levels and wave functions are dependent to the state of strain and electric field produced during the growing process of QDs in a semiconductor substrate. The calculation of the strain and electric field is one of the most challenging components in the QDs simulation process. It involves material anisotropy induced coupling between the elastic and electric fields and it must include the full three-dimensional and usually intricate shapes of the QDs. Numerical simulations are often performed by finite difference, finite element, or atomistic techniques, all require substantial computational time and memory. In this paper, we present a new Green's function approach which takes into account QDs of arbitrary shape and semiconductor substrates with the most general class of anisotropy and piezoelectricity. Following the literature of micromechanics, the problem is formulated as an Eshelby inclusion problem of which the solution can be expressed by a volume-integral equation that involves the Green's functions and the equivalent body-force of eiegenstrain. The volume integral is subsequently reduced to a line integral based on exploiting a unique structure of the Green's functions. The final equations are cast in a form that most of the computational results can be repeatedly used for QDs at different locations—a very attractive feature for simulating large systems of QD arrays. The proposed algorithm has been implemented and validated by comparison with analytical solutions. Numerical simulations are presented for pyramidal QDs in the substrates of gallium arsenide (GaAs) (0 0 1).

Keywords: Self-organized quantum dots; Three-dimensional QDs of arbitrary shape and semiconductor substrates with the most general anisotropy and piezoelectricity; The Green's functions

1. Introduction

The QDs growth technology has advanced to a stage that the self organized QD structures can be produced with high quality in a wide range of semiconductor compounds (Figs. 1 and 2). This has translated into immense interests in research to understand the fundamental physics, as well as an enormous investment in

* Corresponding author. Currently on Sabbatical at Tsinghua University, China.
E-mail addresses: wang20@slb.com (C.-Y. Wang), denda@jove.rutgers.edu (M. Denda), pan2@uakron.edu (E. Pan).

0020-7683/$ - see front matter © 2006 Elsevier Ltd. All rights reserved.
doi:10.1016/j.ijsolstr.2006.03.019

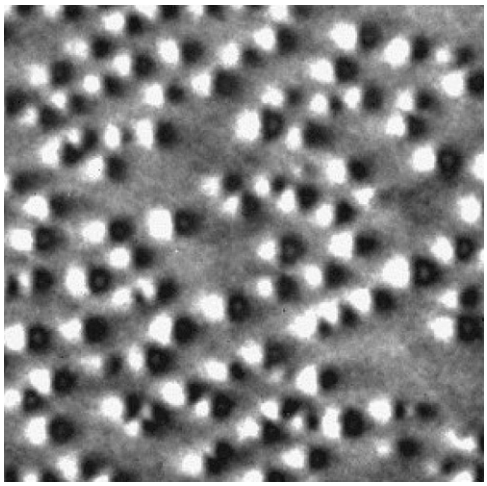

Fig. 1. Micrograph of pyramid-shaped quantum dots grown from indium, gallium, and arsenic. Each dot is about 20 nm wide and 8 nm in height. Image courtesy NIST.

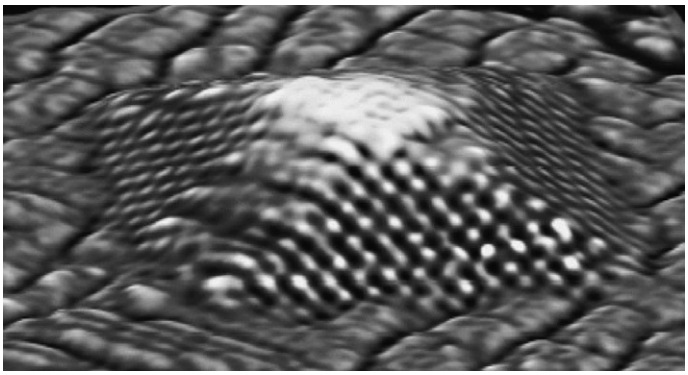

Fig. 2. STM of quantum dot formed by self-assembling (Ge 'pyramid'). Courtesy Hewlett-Packard; image acquired by G. Medeiros-Ribeiro, Hewlett-Packard Labs.

the development of nanotechnology. The quantum effects due to confinement on electronic motion are foreign phenomena to natural materials. It is widely anticipated that the quantum effects and other special electronic and optical properties of QDs will render novel devices with fascinating functionalities and applications. One technology particularly attractive to the petroleum industry is the application in semiconductor light-emitting and laser diodes. Nanotechnology based laser has demonstrated very good temperature characteristics – potentially excellent light sources for downhole optical telemetry and sensing (Fu et al., 2001; Grundmann et al., 1994; Lin, 2001; Martinet et al., 2000; Shim et al., 2002).

Obviously mathematical and numerical simulations have an important role in the study of QDs. At the research stage of exploring the physics, computational simulation is instrumental in interpreting data, and guiding future developments. At the engineering stage of optimization, it provides quantitative analysis quickly and economically that experiments or other means cannot. Analysis of the electronic structure of QDs includes calculations of the electron and hole energy levels and wave functions in arbitrary-shaped QD structures. In addition, it is necessary to take into account effects of the strain and piezoelectric fields induced during the process of QDs growth. Often the growth of semiconductor quantum dots is achieved by the controlled coarsening of a thin film that is strained with respect to the substrate. This self-assembled coarsening/roughening is a result of misfit-lattice-induced strains. The dots are often capped by the substrate material, thus extending the strain around the dot to all angular directions. Not surprisingly, the electronic structure of QDs is profoundly affected by their strain profile. Furthermore, should the semiconductor be

piezoelectric, a misfit-lattice-induced electric potential will also contribute to the properties of the QDs. Indeed one could control/optimize the electronic and optical properties of QDs by altering the elastic strain and electric field (Constantin et al., 2000; Lelarge et al., 1999; Martinet et al., 2000; Medeiros-Ribeiro, 2002; Notomi et al., 1995). The calculation of the strain tensor and electric field is one of the most challenging components in the QD simulation process. It involves material anisotropy induced coupling between the elastic and electric fields and it must include the full three-dimensional and usually intricate shapes of the QDs. Various computational methods with different degrees of sophistication and limitations have been proposed in the last few years. The finite element method (FEM) and finite difference method (FDM) are the most frequently used (Benabbas et al., 1996; Grundmann et al., 1995; Kret et al., 1999; Romanov et al., 2001; Johnson and Freund, 2001). Other methods include the two-dimensional Fourier transform method (Andreev et al., 1999; Holy et al., 1999), the atomistic quantum-mechanics model (Kikuchi et al., 2001; Pryor et al., 1998), and the Green's function methods (Faux and Pearson, 2000; Chu and Wang, 2005). Among them, the Green's function method appears attractive. Its analytical nature provides insights to the understanding of the physics involved. It also produces very accurate numerical solutions with a speed usually faster than the FEM and FDM (Davies, 1998; Faux and Pearson, 2000; Pearson and Faux, 2000). Recently, Pan and his co-workers have employed the equivalent body-force concept of Eshelby inclusion problem (Eshelby, 1957; Mura, 1987). They succeeded in extending the Green's function approach to anisotropic semiconductor substrates (Jogai et al., 2003; Pan and Yang, 2001, 2003; Pan, 2002a,b; Yang and Pan, 2003).

In this paper, we present a new Green's function approach which takes into account QDs of arbitrary shape and semiconductor substrates with the most general class of anisotropy and piezoelectricity. We neglect the size dependent effects that may become important at the scale of a few nanometers (Zhang and Sharma, 2005) and use the size independent classical elasticity. Following Pan (2002a), the problem is formulated as an Eshelby inclusion problem of which the solution can be expressed by a volume-integral equation that involves the Green's functions and the equivalent body-force of eiegenstrain. The volume integral is subsequently reduced to a line integral based on exploiting a unique structure of the Green's functions. The final equations are cast in a form that most of the computational results can be repeatedly used for QDs at different locations—a very attractive feature for simulating large systems of QD arrays. This work can be considered as an improvement of the Green's function approach in computation time and in the inclusion of three-dimensional QDs of arbitrary shapes in a semiconductor substrate of general anisotropy and piezoelectricity. The proposed algorithm has been implemented and validated by comparison with analytical solutions. Numerical simulations are presented for pyramidal QDs in the substrates of gallium arsenide (GaAs) (0 0 1).

2. Equivalent body force of eigenstrain

The eigenstrain in an elastic material and its representation by the equivalent body-force are well established in the classical micromechanics (Eshelby, 1961; Mura, 1987). They have been found useful in the study of QD induced elastic-electric field in the piezoelectric substrate (Pan, 2002a,b). In this section we follow the same train of arguments to derive the equivalent body-force of a QD in a piezoelectric substrate of the most general class of anisotropy, in the three-dimensional Cartesian coordinate system $\mathbf{x} = (x_1, x_2, x_3)$.

Before getting into the subject matter, we shall first introduce compact notations for the coupled electric-elastic fields. The elastic field is described by its displacement vector u_j, body force vector f_j, stress tensor σ_{ij}, strain tensor γ_{ij} and eigenstrain tensor γ^*_{ij}. The electric field quantities include the electric potential ϕ, charge q, displacement vector D_j, field vector E_j, and eigenfield vector E^*_j. We shall adopt the usual compact notations of using capital-letter subscripts for the 'extended' displacement u_J, body force f_J, stress σ_{iJ}, strain γ_{Ji} and eigenstrain γ^*_{Ji} defined as follows (Wang, 1996a,b):

$$u_J = \begin{cases} u_j \\ \phi \end{cases}, \quad f_J = \begin{cases} f_j & J = j = 1,2,3, \\ -q & J = 4 \end{cases} \tag{1}$$

and

$$\sigma_{iJ} = \begin{cases} \sigma_{ij} \\ D_i \end{cases}, \quad \gamma_{Ji} = \begin{cases} \gamma_{ji} \\ E_i \end{cases}, \quad \gamma^*_{Ji} = \begin{cases} \gamma^*_{ji} & J = j = 1,2,3, \\ E^*_i & J = 4. \end{cases} \tag{2}$$

As shown above, a capital-letter subscript indicates an 'extended' elastic-electric field quantity with four components. This is an efficient notation in putting equations in compact forms.

Let γ^*_{Kl} be the extended eigenstrain of the QD defined over a domain V bounded by its boundary ∂V. The extended stress is determined by the constitutive equations

$$\sigma_{iJ} = c_{iJKl}(\gamma_{Kl} - \gamma^*_{Kl}), \tag{3}$$

where the material constants c_{iJKl} are given by

$$c_{iJKl} = \begin{cases} c_{ijkl}, & J = j = 1,2,3, \quad K = k = 1,2,3 \\ e_{kli}, & J = 4, \qquad\quad K = k = 1,2,3 \\ e_{jil}, & K = 4, \qquad\quad J = j = 1,2,3 \\ -\kappa_{il}, & J = K = 4, \end{cases} \tag{4}$$

in which c_{ijkl}, e_{ijk} and κ_{ik} are the elasticity tensor, the piezoelectric tensor and the dielectric permittivity tensor, respectively. The symmetry of the extended fields leads to the symmetry of c_{ijkl}, e_{ijk} and κ_{ik}. Furthermore, a positive extended strain energy requires that c_{ijkl} and κ_{ik} be positive definite. Upon substitution of the following relationships between u_j and γ_{kl} and between ϕ and E_l:

$$\gamma_{kl} = (u_{k,l} + u_{l,k})/2, \quad E_l = \phi_{,l}, \tag{5}$$

the constitutive equations (3) yield

$$\sigma_{iJ} = c_{iJKl}(u_{K,l} - \gamma^*_{Kl}), \tag{6}$$

where the following symmetry conditions have been used

$$c_{ijkl} = c_{jikl} = c_{ijlk} = c_{klij}, \quad e_{ijk} = e_{jik}, \quad \kappa_{ij} = \kappa_{ji}. \tag{7}$$

In this paper, $\partial_i f$ or $f_{,i}$ is used to indicate partial derivative of $f(\mathbf{x})$ with respect to x_i. The summation convention over repeated indices is applied.

Now, substitution of (6) into the equilibrium equations

$$\sigma_{iJ,i} = 0 \tag{8}$$

leads to

$$c_{iJKl}\partial_l\partial_i u_K = c_{iJKl}\gamma^*_{Kl,i}. \tag{9}$$

The term in the right-hand side

$$f_J(\mathbf{x}) = -c_{iJKl}\gamma^*_{Kl,i}(\mathbf{x}) \tag{10}$$

is the equivalent body force of the eigenstrain γ^*_{Kl} (Mura, 1987; Pan, 2002b) defined in the QD domain V.

3. Volume and boundary integral expressions

Eq. (9) lends itself directly to the volume integral representation

$$u_P(\mathbf{y}) = -\int_V g_{JP}(\mathbf{x},\mathbf{y})[c_{iJLm}\gamma^*_{Lm}]_{,i}\,\mathrm{d}V(\mathbf{x}), \tag{11}$$

where $g_{JP}(\mathbf{x},\mathbf{y})$ is the Green's function, which is the singular displacement solution produced by a point source. Specifically, $g_{JP}(\mathbf{x},\mathbf{y})$ corresponds to the Jth component of the extended displacement at location $\mathbf{x}$ produced by the Pth component of an extended point force applied at $\mathbf{y}$. If we assume that the eigenstrain is uniform within the QD domain V, the volume integral (11) can be transformed into a surface integral on the boundary ∂V, following the framework of Mura (1987) or its extension to the piezoelectricity of Pan (2002b). The result is

$$u_P(\mathbf{y}) = c_{iJLm}\gamma^*_{Lm}\int_{\partial V} g_{JP}(\mathbf{x},\mathbf{y})n_i(\mathbf{x})\,\mathrm{d}s(\mathbf{x}), \tag{12}$$

where $n_i(\mathbf{x})$ is the outward normal to the boundary ∂V.

In what follows, we shall first derive a line integral expression for the Green's function g_{JP} following Wang and Achenbach (1995), and then evaluate the surface integral (12) analytically.

4. Green's functions

The Green's functions $g_{PM}(\mathbf{x})$ is the solution of the singular partial differential equation

$$\Gamma_{JP}(\partial_{\mathbf{x}})g_{PM}(\mathbf{x}-\mathbf{y}) = -\delta_{JM}\delta(\mathbf{x}-\mathbf{y}), \tag{13}$$

where Γ_{JP} is the differential operator

$$\Gamma_{JP}(\partial_{\mathbf{x}}) = c_{iJPq}\partial_i\partial_l, \tag{14}$$

and δ_{JM} is the Kronecker delta. Using the identity of delta function $\delta(\mathbf{x})$:

$$\frac{-1}{8\pi^2}\Delta\int_{|\mathbf{d}|=1}\delta[\mathbf{d}\cdot(\mathbf{x}-\mathbf{y})]\,\mathrm{d}\Omega(\mathbf{d}) = \delta(\mathbf{x}-\mathbf{y}), \tag{15}$$

it is easily verified that (13) is satisfied by

$$g_{JP}(\mathbf{x},\mathbf{y}) = \frac{1}{8\pi^2}\int_{|\mathbf{d}|=1}\frac{A_{JP}(\mathbf{d})}{D(\mathbf{d})}\delta[\mathbf{d}\cdot(\mathbf{x}-\mathbf{y})]\,\mathrm{d}\Omega(\mathbf{d}), \tag{16}$$

where

$$A_{JP}(\mathbf{d}) = \mathrm{adj}\ \Gamma_{JP}(\mathbf{d}), \quad D(\mathbf{d}) = \det\Gamma_{JP}(\mathbf{d}). \tag{17}$$

Let $(\mathbf{e}^1, \mathbf{e}^2, \mathbf{n})$ be a set of unit orthogonal base vectors (for now, we consider $\mathbf{n}$ as a constant unit vector, it will be used later as the outward normal to the boundary ∂V). We express the unit sphere $|\mathbf{d}| = 1$ by

$$\mathbf{d} = \sin\phi\cos\theta\ \mathbf{e}^1 + \sin\phi\sin\theta\ \mathbf{e}^2 + \cos\phi\mathbf{n}, \tag{18}$$

and change integral (16) to

$$g_{JP}(\mathbf{x}-\mathbf{y}) = \frac{1}{4\pi^2}\int_0^{\pi}\int_0^{\pi}\frac{A_{JP}(\mathbf{d})}{D(\mathbf{d})}\delta[\mathbf{d}\cdot(\mathbf{x}-\mathbf{y})]\sin\phi\,\mathrm{d}\phi\,\mathrm{d}\theta. \tag{19}$$

In deriving the above equation, symmetry with respect to θ and ϕ has been used. A subsequent substitution of $\eta = \cot(\phi)$ leads to

$$g_{JP}(\mathbf{x}-\mathbf{y}) = \frac{1}{4\pi^2}\int_0^{\pi}\int_{-\infty}^{\infty}\frac{A_{JP}(\mathbf{s})}{D(\mathbf{s})}\delta[\mathbf{s}\cdot(\mathbf{x}-\mathbf{y})]\,\mathrm{d}\eta\,\mathrm{d}\theta, \tag{20}$$

where

$$\mathbf{s} = \cos\theta\ \mathbf{e}^1 + \sin\theta\ \mathbf{e}^2 + \eta\mathbf{n}. \tag{21}$$

Since (Gel'fand et al., 1966)

$$\left(\frac{1}{x+\mathrm{i}\gamma}\right) = \wp\frac{1}{x} - \mathrm{i}\,\mathrm{sign}(\gamma)\pi\delta(x), \quad \text{for } \gamma\to 0, \tag{22}$$

where $\wp$ indicates the principle part, we have

$$\delta(x) = \frac{-\mathrm{sign}(\gamma)}{\pi}\Im\left(\frac{1}{x+\mathrm{i}\gamma}\right), \quad \text{for } \gamma\to 0, \tag{23}$$

where $\Im$ indicates the imaginary part. Hence, we have

$$g_{JP}(\mathbf{x},\mathbf{y}) = \frac{-\mathrm{sign}(\gamma)}{4\pi^3}\Im\int_0^{\pi}\int_{-\infty}^{\infty}\frac{A_{JP}(\mathbf{s})}{D(\mathbf{s})}\frac{\mathrm{d}\eta\mathrm{d}\theta}{\mathbf{s}\cdot(\mathbf{x}-\mathbf{y})+\mathrm{i}\gamma}, \quad \text{for } \gamma\to 0. \tag{24}$$

The positive definiteness of c_{ijkl} and κ_{ik} guarantees that the system of partial differential equations (13) is strictly elliptical, and that roots of the characteristic equation $D = 0$, where D is the determinant defined by

(17), cannot be real-valued (Deeg, 1980; Dunn, 1994). That together with the fact that $D(\mathbf{s})$ is a polynomial with real coefficients permit us to write

$$D(\mathbf{s}) = d_8\eta^8 + d_7\eta^7 + \cdots + d_0 = d_8\prod_{\kappa=1}^{4}(\eta-\eta_\kappa)(\eta-\bar{\eta}_\kappa), \tag{25}$$

where $d_i(\theta)$ are the real-valued coefficients, $\eta_\kappa(\theta)$ are roots of $D=0$ with positive imaginary parts (i.e, $\Im(\eta_\kappa)>0$), and $\bar{\eta}_\kappa$ are complex conjugates of η_κ.

Now, based on Cauchy's residue theorem, integration in (24) with respect to η yields residues at $\eta=\eta_\kappa$. The result is

$$g_{JP}(\mathbf{x},\mathbf{y}) = -\Re\int_0^\pi \sum_{\kappa=1}^{4}\bar{g}^\kappa_{JP}(\theta)\frac{\operatorname{sign}[\mathbf{n}\cdot(\mathbf{x}-\mathbf{y})]}{\mathbf{s}^\kappa\cdot(\mathbf{x}-\mathbf{y})}\,\mathrm{d}\theta, \tag{26}$$

where

$$\mathbf{s}^\kappa = \cos\theta\ \mathbf{e}^1 + \sin\theta\ \mathbf{e}^2 + \eta_\kappa\mathbf{n}, \tag{27}$$

and

$$\bar{g}^\kappa_{JP}(\theta) = \frac{1}{2\pi^2}\frac{A_{JP}(\mathbf{s}^\kappa)}{D_{,\eta}(\mathbf{s}^\kappa)}. \tag{28}$$

In the above expression,

$$D_{,\eta}(\mathbf{s}^\kappa) \equiv \frac{\partial}{\partial\eta}D(\mathbf{s})_{(\eta=\eta_\kappa)} = \left[\sum_{m=1}^{8} m d_m \eta^{(m-1)}\right]_{(\eta=\eta_\kappa)} = d_8(\eta_\kappa-\bar{\eta}_\kappa)\prod_{(q=1)(q\neq\kappa)}^{4}(\eta-\eta_q)(\eta-\bar{\eta}_q). \tag{29}$$

Following the procedure presented above, we can also obtain

$$g_{JP,q}(\mathbf{x},\mathbf{y}) = \Re\int_0^\pi \sum_{k=1}^{4} s^\kappa_q\bar{g}^\kappa_{JP}(\theta)\frac{\operatorname{sign}[\mathbf{n}\cdot(\mathbf{x}-\mathbf{y})]}{[\mathbf{s}^\kappa\cdot(\mathbf{x}-\mathbf{y})]^2}\,\mathrm{d}\theta. \tag{30}$$

We notice the integrand of the line integral (26) is given by the product of two terms, $\bar{g}^k_{jp}(\theta)$ and $\operatorname{sign}[\mathbf{n}\cdot(\mathbf{x}-\mathbf{y})]/\mathbf{s}^k\cdot(\mathbf{x}-\mathbf{y})$. The first term, $\bar{g}^k_{jp}(\theta)$, given by (28) is a function of the material properties only, i.e., independent to the location vectors $\mathbf{x}$ and $\mathbf{y}$. The second term, $\operatorname{sign}[\mathbf{n}\cdot(\mathbf{x}-\mathbf{y})]/\mathbf{s}^k\cdot(\mathbf{x}-\mathbf{y})$, is a simple algebraic function. It is in fact a 'plane wave function' which is in essence a one-dimensional function. We exploit the simple structure of the integrands in (26) and (30) in our evaluation of these integrals.

5. Evaluation for quantum dots of arbitrary shapes

5.1. Exchange of integration order

We proceed to evaluate the boundary integral (12) using the line integral expressions for the Green's functions (26) and (30). We consider a QD of arbitrary shape, but we assume the QD surface can be effectively represented or approximated by a number of triangular surfaces. It is therefore sufficient to consider integral (12) over a triangular surface A:

$$u_P(\mathbf{y}) = c_{iJLm}\gamma^*_{Lm}n_i\int_A g_{JP}(\mathbf{x},\mathbf{y})\,\mathrm{d}A(\mathbf{x}), \tag{31}$$

where $\mathbf{n}$ is the outward normal to A. From (5) and (31), it is straightforward to derive the QD induced strain field

$$\gamma_{pq}(\mathbf{y}) = \frac{1}{2}c_{iJLm}\gamma^*_{Lm}n_i\int_A [g_{Jq,p}(\mathbf{x},\mathbf{y}) + g_{Jp,q}(\mathbf{x},\mathbf{y})]\,\mathrm{d}A(\mathbf{x}), \tag{32}$$

and the QD induced electric filed

$$E_p(\mathbf{y}) = c_{iJLm}\gamma^*_{Lm}n_i \int_A g_{J4,p}(\mathbf{x},\mathbf{y})\,\mathrm{d}A(\mathbf{x}). \tag{33}$$

Substituting solutions (26) and (30) into (31)–(33), and exchanging integration orders, we obtain

$$u_P(\mathbf{y}) = c_{iJLm}\gamma^*_{Lm}n_i \int_0^\pi \Re \sum_{k=1}^{4} \bar{g}^{\kappa}_{JP}(\theta)\phi_\kappa(\mathbf{y},\theta)\,\mathrm{d}\theta, \tag{34}$$

$$\gamma_{pq}(\mathbf{y}) = \frac{1}{2}c_{iJLm}\gamma^*_{Lm}n_i \int_0^\pi \Re \sum_{k=1}^{4} [s^{\kappa}_q \bar{g}^{\kappa}_{Jp}(\theta) + s^{\kappa}_p \bar{g}^{\kappa}_{Jq}(\theta)]\psi_\kappa(\mathbf{y},\theta)\,\mathrm{d}\theta, \tag{35}$$

and

$$E_p(\mathbf{y}) = c_{iJLm}\gamma^*_{Lm}n_i \int_0^\pi \Re \sum_{k=1}^{4} s^{\kappa}_p \bar{g}^{\kappa}_{J4}(\theta)\psi_\kappa(\mathbf{y},\theta)\,\mathrm{d}\theta, \tag{36}$$

where

$$\phi_\kappa(\mathbf{y},\theta) = -\int_A \frac{\mathrm{sign}[\mathbf{n}\cdot(\mathbf{x}-\mathbf{y})]\,\mathrm{d}A(\mathbf{x})}{\mathbf{s}^\kappa\cdot[\mathbf{x}-\mathbf{y}]}, \tag{37}$$

and

$$\psi_\kappa(\mathbf{y},\theta) = \int_A \frac{\mathrm{sign}[\mathbf{n}\cdot(\mathbf{x}-\mathbf{y})]\,\mathrm{d}A(\mathbf{x})}{\{\mathbf{s}^\kappa\cdot[\mathbf{x}-\mathbf{y}]\}^2}. \tag{38}$$

The above two surface integrals (37) and (38) over A can be integrated analytically. As a result, only the line integrals over $(0,\pi/2)$ in Eqs. (34)–(36) need to be computed numerically.

5.2. Geometry and local coordinates of triangular element

To carry out the integration of integrals (37) and (38), we shall first set up local coordinates for the triangular element A. Referring to Figs. 3 and 4, let us number the three nodes of the element, ($\mathbf{x}^{(1)}$, $\mathbf{x}^{(2)}$, and $\mathbf{x}^{(3)}$), counterclockwise around the outward normal vector $\mathbf{n}$, such that

$$\mathbf{n} = \frac{(\mathbf{x}^{(2)}-\mathbf{x}^{(1)})\times(\mathbf{x}^{(3)}-\mathbf{x}^{(2)})}{2\Delta} = \frac{(\mathbf{x}^{(3)}-\mathbf{x}^{(2)})\times(\mathbf{x}^{(1)}-\mathbf{x}^{(3)})}{2\Delta} = \frac{(\mathbf{x}^{(1)}-\mathbf{x}^{(3)})\times(\mathbf{x}^{(2)}-\mathbf{x}^{(1)})}{2\Delta}, \tag{39}$$

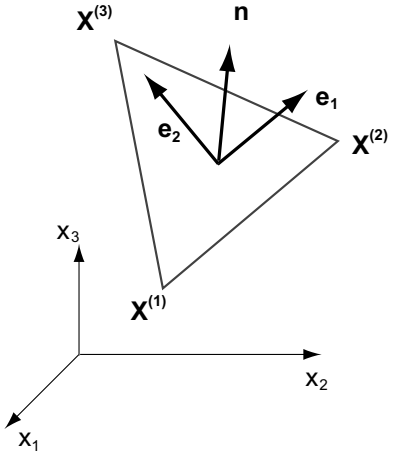

Fig. 3. Geometry of the triangular element A. Three nodes $\mathbf{x}^{(1)}\mathbf{x}^{(2)}\mathbf{x}^{(3)}$ and the local orthogonal base vectors ($\mathbf{e}_1$, $\mathbf{e}_2$, $\mathbf{n}$), where $\mathbf{e}_1$ $\mathbf{e}_2$ are an arbitrary pair of orthogonal vectors on in the plane of A and $\mathbf{n}$ is the unit normal to A.

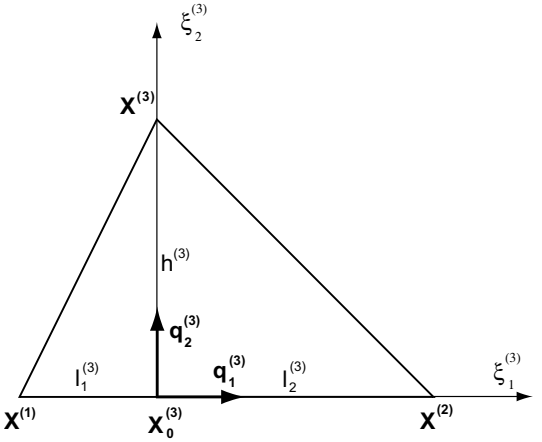

Fig. 4. Local coordinate system $(\xi_1^{(n)}, \xi_2^{(n)}, \xi_3)$ with the unit vectors $\mathbf{q}_1^{(n)}$ and $\mathbf{q}_2^{(n)}$ and $\mathbf{n}$, where $n = 3$ in this figure. The axis ξ_3 and the unit normal $\mathbf{n}$, perpendicular to the element, are not shown.

where Δ is the area of the triangular element A. Let

$$\mathbf{q}_1 = \frac{\mathbf{x}^{(2)} - \mathbf{x}^{(1)}}{|\mathbf{x}^2 - \mathbf{x}^{(1)}|}, \quad \mathbf{q}_2 = \mathbf{n} \times \mathbf{q}_1, \tag{40}$$

as shown in Fig. 4, where $\mathbf{q}_1$ is in the direction of the element edge located across from the third node $\mathbf{x}^{(3)}$. We use $(\mathbf{q}_1, \mathbf{q}_2, \mathbf{n})$ as the unit orthogonal base vectors for local coordinates (ξ_1, ξ_2, ξ_3). The transformation between the global and the local coordinates is given by

$$\mathbf{x} = \mathbf{x}_0 + \xi_1 \mathbf{q}_1 + \xi_2 \mathbf{q}_2 + \xi_3 \mathbf{n}, \tag{41}$$

with the coordinate origin $\mathbf{x}_0$ (Figs. 3 and 4)

$$\mathbf{x}_0 = \mathbf{x}^{(1)} + [(\mathbf{x}^{(3)} - \mathbf{x}^{(1)}) \cdot \mathbf{q}_1]\mathbf{q}_1 = \mathbf{x}^{(3)} - [(\mathbf{x}^{(3)} - \mathbf{x}^{(1)}) \cdot \mathbf{q}_2]\mathbf{q}_2. \tag{42}$$

We shall also introduce the following geometrical quantities (Fig. 4)

$$h = (\mathbf{x}^{(3)} - \mathbf{x}^{(1)}) \cdot \mathbf{q}_2, \quad l = |\mathbf{x}^{(2)} - \mathbf{x}^{(1)}|, \quad l_1 = (\mathbf{x}^3 - \mathbf{x}^{(1)}) \cdot \mathbf{q}_1, \quad l_2 = l - l_1. \tag{43}$$

In the local coordinates, the location vector $\mathbf{y}$ is expressed by

$$\mathbf{y} = \mathbf{x}_0 + \tilde{y}_1 \ \mathbf{q}_1 + \tilde{y}_2 \ \mathbf{q}_2 + \tilde{y}_3 \ \mathbf{n}, \tag{44}$$

where

$$\tilde{y}_1 = (\mathbf{y} - \mathbf{x}_0) \cdot \mathbf{q}_1, \quad \tilde{y}_2 = (\mathbf{y} - \mathbf{x}_0) \cdot \mathbf{q}_2, \quad \tilde{y}_3 = (\mathbf{y} - \mathbf{x}_0) \cdot \mathbf{n}. \tag{45}$$

Recall that $(\mathbf{e}^1, \mathbf{e}^2, \mathbf{n})$ and $(\mathbf{q}_1, \mathbf{q}_2, \mathbf{n})$ are both unit orthogonal base vectors. Henceforth, using Eqs. (27), (41) and (44), we get

$$\mathbf{s}^\kappa \cdot (\mathbf{x} - \mathbf{y}) = (\xi_1 - \tilde{y}_1)\cos(\theta - \alpha) + (\xi_2 - \tilde{y}_2)\sin(\theta - \alpha) + (\xi_3 - \tilde{y}_3)\eta_\kappa, \tag{46}$$

where α, the angle between $\mathbf{q}_1$ and $\mathbf{e}_1$, is determined by

$$\cos\alpha = \mathbf{e}_1 \cdot \mathbf{q}_1 = \mathbf{e}_2 \cdot \mathbf{q}_2, \quad \sin\ \alpha = -\mathbf{e}_2 \cdot \mathbf{q}_1 = \mathbf{e}_1 \cdot \mathbf{q}_2. \tag{47}$$

5.3. Analytical solutions of ϕ and ψ

Substitution of (46) into integral (37) yields

$$\phi_\kappa(\mathbf{y}, \beta) = \text{sign}(y_3) \int_0^h \int_{-l_1 + l_1\xi_2/h}^{l_2 - l_2\xi_2/h} \frac{\mathrm{d}\xi_1 \mathrm{d}\xi_2}{\xi_1 \cos\beta + \xi_2 \sin\beta - \varsigma_\kappa}, \tag{48}$$

where

$$\beta = \theta - \alpha, \tag{49}$$

and

$$\varsigma_\kappa = \tilde{y}_1 \cos\beta + \tilde{y}_2 \sin\beta + \tilde{y}_3 \eta_\kappa. \tag{50}$$

In writing expression (48), $\xi_3 = 0$ for $\mathbf{x} \in A$ has been considered. By a straightforward integration of (48), we obtain

$$\phi_\kappa(\mathbf{y}, \beta) = \frac{\operatorname{sign}(y_3) h}{\cos\ \beta} \left[\frac{z_1 \log z_1 - z_2 \log z_2}{z_1 - z_2} - \frac{z_1 \log z_1 - z_3 \log z_3}{z_1 - z_3} \right], \tag{51}$$

where

$$z_1 = h \sin\beta - \varsigma_\kappa, \quad z_2 = l_2 \cos\beta - \varsigma_\kappa, \quad z_3 = -l_1 \cos\beta - \varsigma_\kappa. \tag{52}$$

Similarly, upon substitution of (46), integral (38) becomes

$$\psi_\kappa(\mathbf{y}, \beta) = -\operatorname{sign}(y_3) \int_0^h \int_{-l_1 + l_1 \xi_2/h}^{l_2 - l_2 \xi_2/h} \frac{\mathrm{d}\xi_1 \mathrm{d}\xi_2}{(\xi_1 \cos\beta + \xi_2 \sin\beta - \varsigma_\kappa)^2}, \tag{53}$$

which can be evaluated analytically to give

$$\psi_\kappa(\mathbf{y}, \beta) = \frac{\operatorname{sign}(y_3) h}{\cos\beta} \left[\frac{\log z_1 - \log z_2}{z_1 - z_2} - \frac{\log z_1 - \log z_3}{z_1 - z_3} \right]. \tag{54}$$

Now, with the analytical solutions given by (51) and (54), the only concerns remained are the computation of the three line integrals (34)–(36), which can be achieved by numerical integration. We observe that the integrands of expressions (48) and (53) are regular functions and hence ϕ_κ and ψ_κ are regular, when imaginary part of ς_κ does not vanish. From Eq. (50) we find that $\Im\varsigma_\kappa = 0$ only when $\tilde{y}_3 = 0$. Therefore we conclude, when $\tilde{y}_3 \neq 0$, i.e., when $\mathbf{y}$ is not on the plane of the triangular surface A, $\phi_\kappa(\mathbf{y}, \beta)$ and $\psi_\kappa(\mathbf{y},\beta)$ are regular functions of β and thus so are the integrands of the line integrals (34)–(36).

Eqs. (51) and (54) together with the three line integral equations (34)–(36) are the key results of this paper. Note that the integrand in the line integral (34) is given by the products of functions $\bar{g}^k_{JP}(\theta)$ and $\phi^{(mn)}_k(\mathbf{y}, \theta)$, where $\bar{g}^k_{JP}(\theta)$ are functions of the material properties only, while $\phi^{(mn)}_k$ are simple algebraic functions of location and geometry. Notice the location and geometry independent term $\bar{g}^k_{JP}(\theta)$, which is more costly to compute than the simple functions $\phi^{(mn)}_k(\mathbf{y}, \theta)$, can be calculated only once and stored to be repeatedly used for QDs at different locations. This unique structure of the integrand facilitates the coding procedure and accelerate the computation for very large systems.

6. Numerical results

The elastic stiffness, the piezoelectric and the dielectric permittivity constants are of the order of 10^{11} (N/m^2), 10^1 (C/m^2) and 10^{-9} (C/(mV)), respectively, and the typical strain and the electric fields are of the order of 10^{-3} and 10^7 (V/m), respectively. Let q and q_0 represent a dimensional quantity and its reference value, respectively; its normalization is given by $\bar{q} = q/q_0$. We select the reference values for the stress, strain, electric induction, and the electric fields to be $\sigma_0 = 10^8$ (N/m^2), $\gamma_0 = 10^{-3}$, $D_0 = 10^{-2}$ (C/m^2), and $E_0 = 10^7$ (V/m), respectively.

For the verification of the code we have calculated the spherical inclusion problem in an infinite isotropic body with Poisson's ratio 0.25. It is known that the strain field inside the ellipsoidal inclusion of constant eigenstrain is uniform and is given by Eshelby's S-tensor according to (Mura, 1987)

$$\gamma_{ij} = S_{ijkl} \gamma^*_{kl}. \tag{55}$$

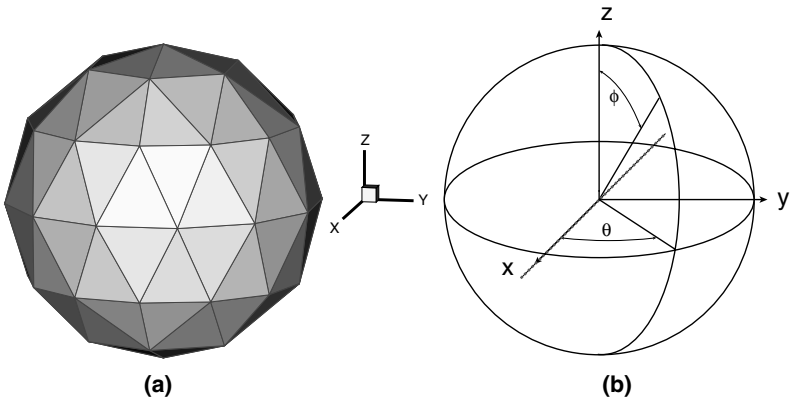

Fig. 5. (a) Discretization of the unit sphere by 96 triangles. (b) Strain components are plotted along the x-axis in and outside of the sphere.

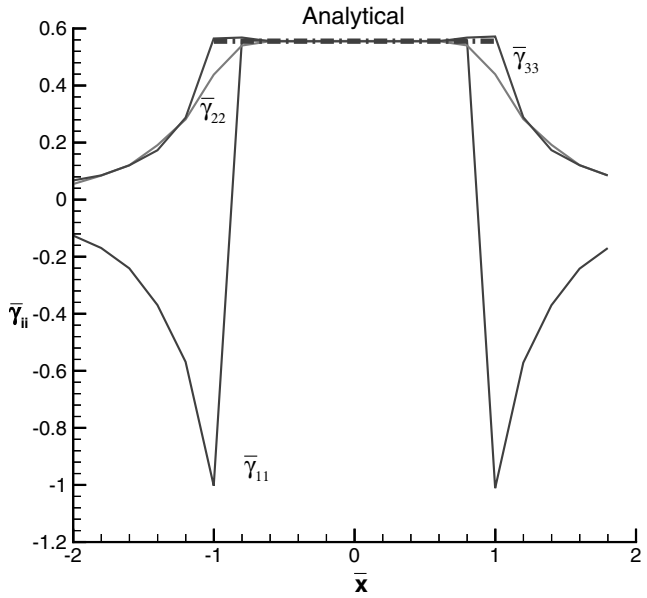

Fig. 6. Variation of strain components $\bar{\gamma}_{11}$, $\bar{\gamma}_{22}$ and $\bar{\gamma}_{33}$ along the x-axis. The analytical values are plotted inside the sphere only.

Fig. 5(a) shows the discretization of the unit sphere by 96 triangles. The uniform non-dimensional eigenstrain components of unit magnitude, $\bar{\gamma}^*_{11} = \bar{\gamma}^*_{22} = \bar{\gamma}^*_{33} = \bar{\gamma}^*_{23} = \bar{\gamma}^*_{31} = \bar{\gamma}^*_{12} = 1$, are given inside the sphere. The plots of the strain variation along the x-axis, as shown in Fig. 5(b), are given in Figs. 6 and 7. Note that the strain components inside the unit sphere are constant and perfectly agree with the analytical values given by (55). The difference between γ_{22} and γ_{33} comes from the difference in the discretization of the sphere in the x_2 and x_3 directions and is not the numerical error. Another verification was made with the cuboidal inclusion in an infinite isotropic body with Poisson's ratio 0.25. Six components of the uniform non-dimensional eigenstrain of the unit magnitude were introduced in the unit cube ($\bar{a} = \bar{b} = \bar{c} = 1$) shown in Fig. 8. The centroid of the cube coincides with the coordinate origin.

Fig. 9(a) shows the variation of the normalized strain component $\bar{\gamma}_{31}$ on the xz-plane where $y = 0$. The corresponding plot of the analytical solution Mura (1987) are given in Fig. 9(b) for comparison. The inclusion region is defined by a rectangle, $-1 \leqslant \bar{x} \leqslant +1$ and $-1 \leqslant \bar{z} \leqslant +1$. Notice that the results obtained by the proposed technique agree perfectly with the analytical results, including those for five other strain components $\bar{\gamma}_{22}$,

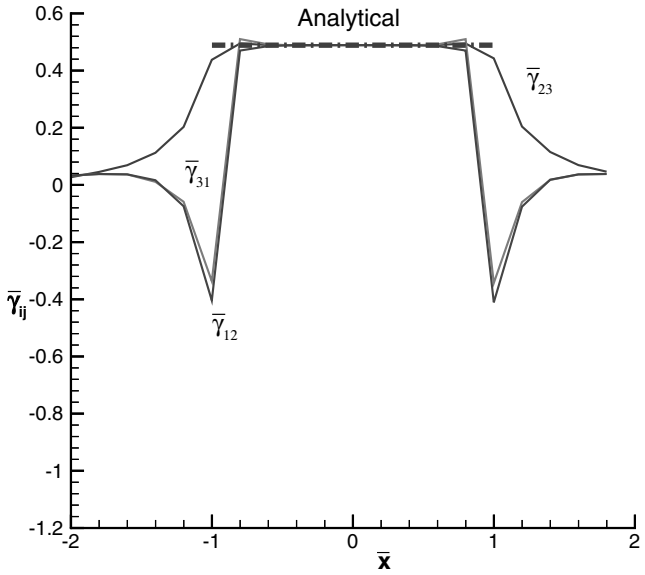

Fig. 7. Variation of strain components $\bar{\gamma}_{23}$, $\bar{\gamma}_{31}$ and $\bar{\gamma}_{12}$ along the x-axis. The analytical values are plotted inside the sphere only.

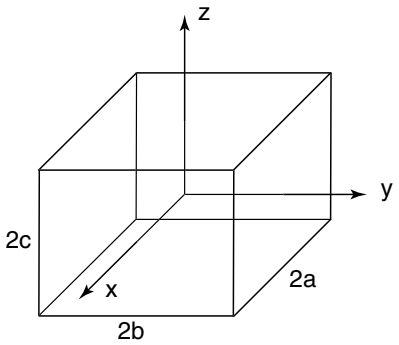

Fig. 8. Cuboidal inclusion with uniform eigenstrain.

$\bar{\gamma}_{11}$, $\bar{\gamma}_{33}$, $\bar{\gamma}_{12}$ and $\bar{\gamma}_{23}$ not shown here. Especially notable is the accurate representation of the logarithmic singularity, as predicted by the analytical solution, at the corners of the cuboid as shown in Fig. 9.

In order to demonstrate the capability of the technique developed for the application to the quantum dots, we have selected a pyramidal inclusion of uniform eigenstrain distribution as shown in Fig. 10. The unit non-dimensional base length $\bar{a} = 1$ and height $\bar{h} = 1$ are specified for the pyramid. Gallium arsenide (0 0 1) (cubic) with the material constants given by

$$[c_{\mathscr{I}\mathscr{J}}/c_0] = \begin{bmatrix} 1.18, & 0.54, & 0.54, & 0.0, & 0.0, & 0.0 \\ & 1.18, & 0.54, & 0.0, & 0.0, & 0.0 \\ & & 1.18, & 0.0, & 0.0, & 0.0 \\ & & & 0.59, & 0.0, & 0.0 \\ & & & & 0.59, & 0.0 \\ & & & & & 0.59 \end{bmatrix},$$

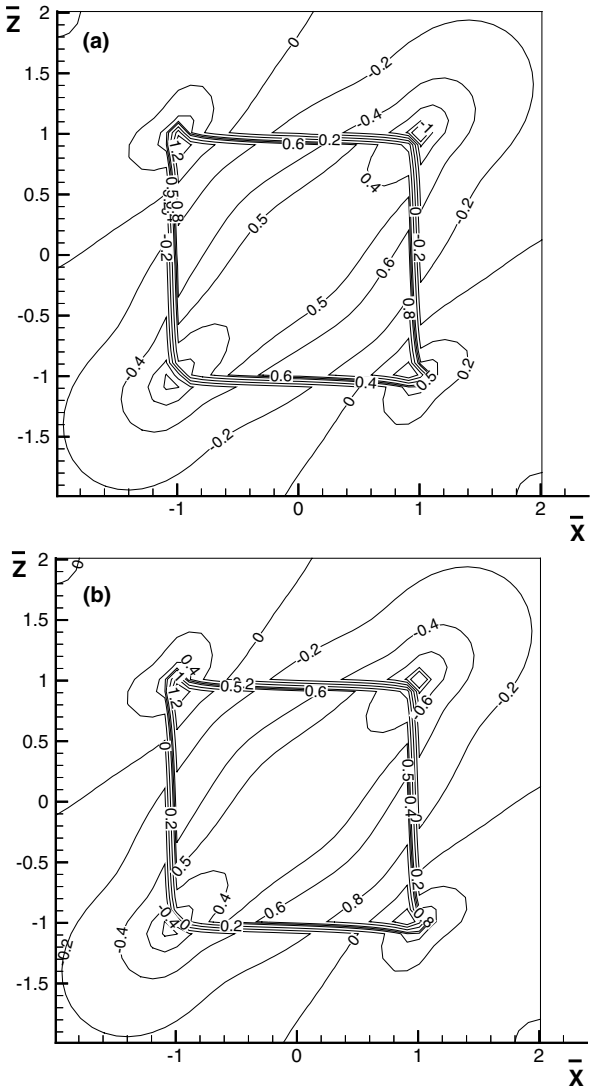

Fig. 9. Distribution of $\bar{\gamma}_{31}$ on the xz-plane through the centroid of the cuboidal inclusion in an isotropic solid. (a) Numerical and (b) analytical results.

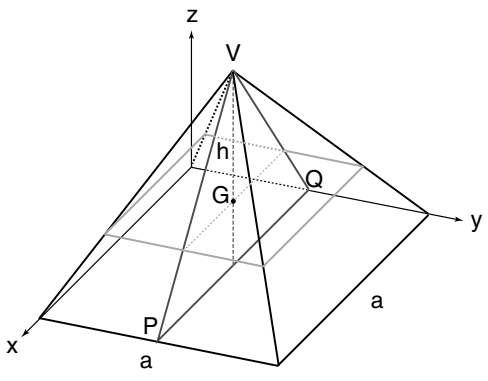

Fig. 10. Pyramidal quantum dot with uniform eigenstrain.

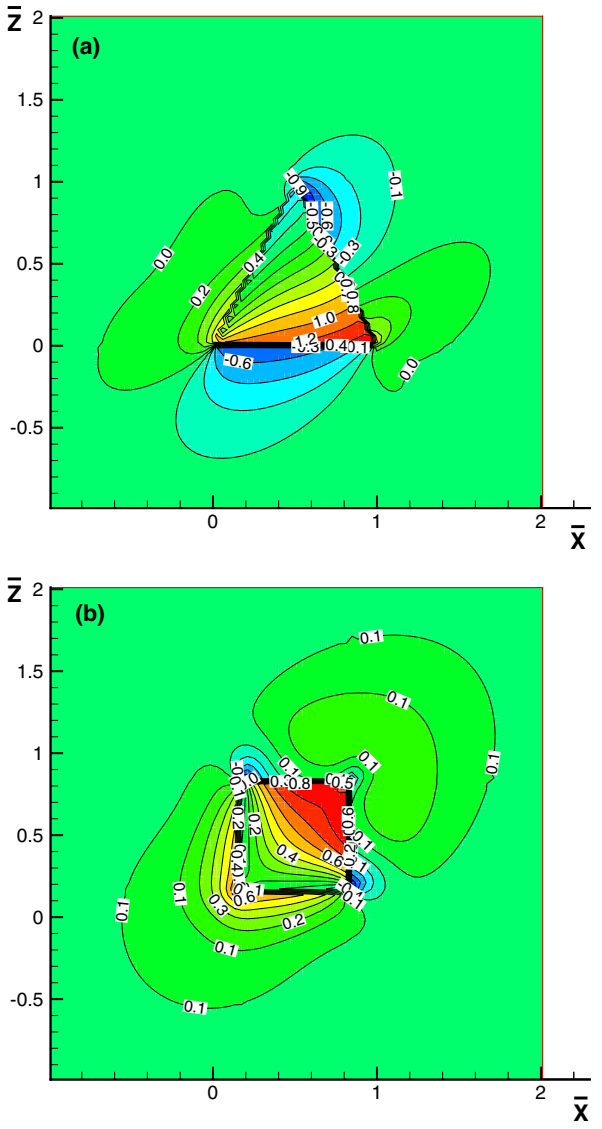

Fig. 11. Pyramidal inclusion in gallium arsenide (001): distribution of $\bar{\gamma}_{33}$ (a) on the vertical plane VPQ and (b) on the horizontal plane through the centroid G of Fig. 10.

$$[e_{\mathscr{I}j}/e_0] = \begin{bmatrix} 0.0, & 0.0, & 0.0, & -0.016, & 0.0, & 0.0 \\ 0.0, & 0.0, & 0.0, & 0.0, & -0.016, & 0.0 \\ 0.0, & 0.0, & 0.0, & 0.0, & 0.0, & -0.016 \end{bmatrix},$$

$$[\kappa_{ij}/(8.854 \times \kappa_0)] = \begin{bmatrix} 0.0125, & 0.0, & 0.0 \\ & 0.0125, & 0.0 \\ & & 0.0125 \end{bmatrix},$$

where $c_0 = 10^{11}$ N/m^2, $e_0 = 10^1$ C/m^2 and $\kappa_0 = 10^{-9}$ C/(mV) is considered. Note that for the stiffness and piezoelectric constants we replace the pair of suffices ij by a single suffix $\mathscr{I}$ according to the convention $(11 \to 1)$, $(22 \to 2)$, $(33 \to 3)$, $(23 \to 4)$, $(31 \to 5,)$ $(12 \to 6)$. The unit non-dimensional eigenstrain components $\bar{\gamma}^*_{ij} = 1$ and $\bar{E}^*_i = 1$ are given inside the pyramid.

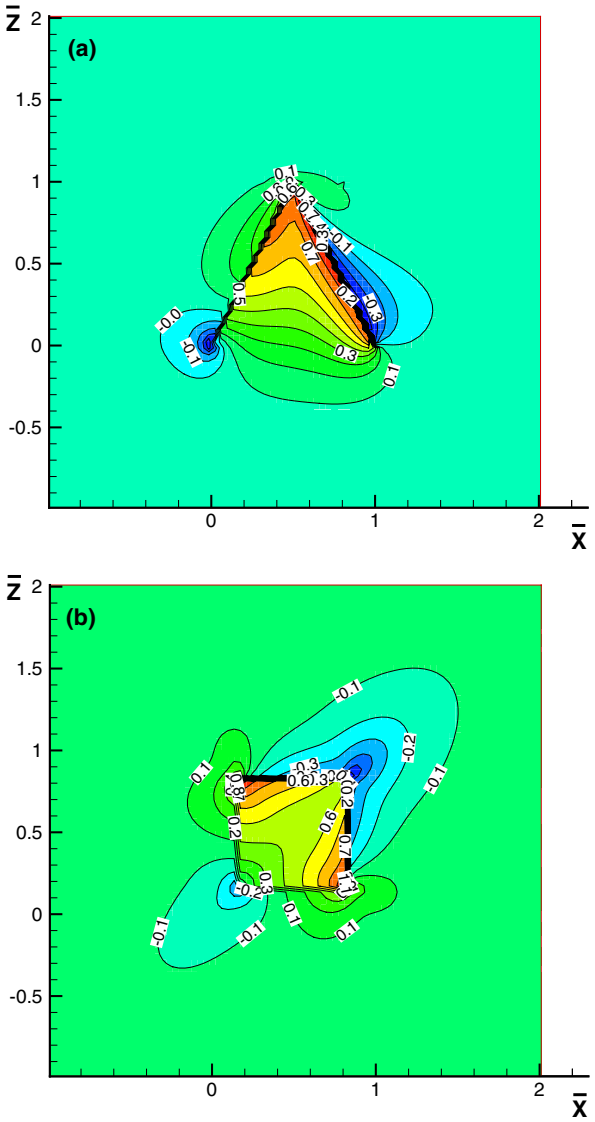

Fig. 12. Pyramidal inclusion in gallium arsenide (0 0 1): distribution of $\bar{\gamma}_{12}$ (a) on the vertical plane VPQ and (b) on the horizontal plane through the centroid G of Fig. 10.

Figs. 11–13 show the distribution of the some components of the extended strain in (a) a vertical plane, parallel to the xz-plane, that cut through the vertex V of the pyramid and (b) on the horizontal plane through the centroid G of the pyramid, as shown in Fig. 10.

7. Summary

In this paper, we have presented a new Green's function approach for the calculation of the strain and electric field in and out of QDs embedded in the semiconductor substrate. We have taken into account QDs of arbitrary shape and semiconductor substrates with the most general class of anisotropy and piezoelectricity. The problem is formulated as an Eshelby inclusion problem of which the solution can be expressed by a volume-integral equation, which is subsequently reduced to a line integral based on exploiting a unique structure of the Green's functions. This unique structure of the integrand of the line integral facilitates the coding procedure and the computation for very large systems. The proposed algorithm has been implemented and

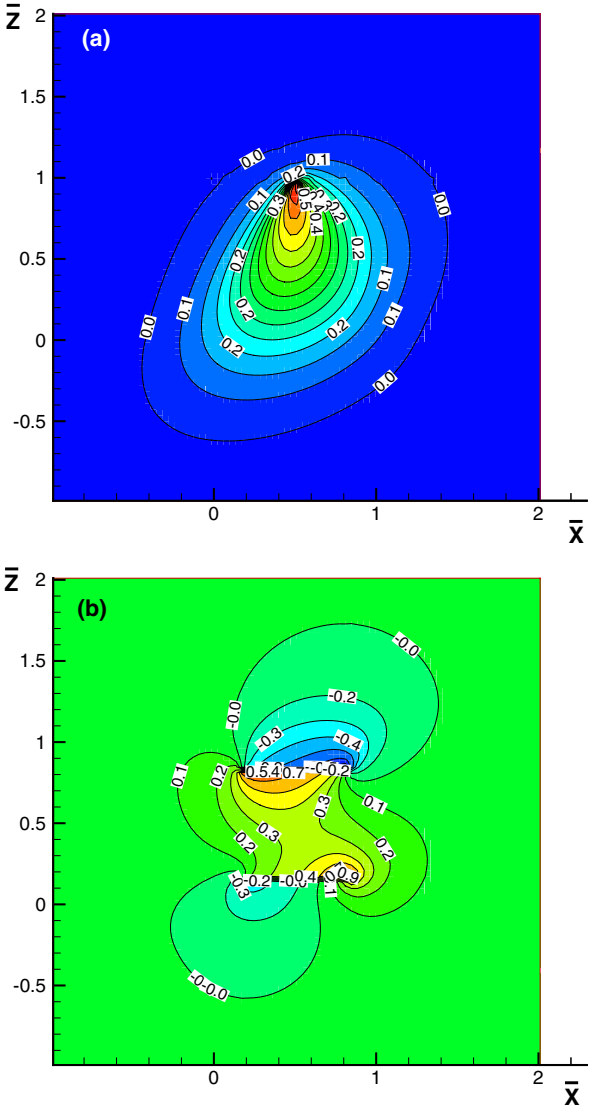

Fig. 13. Pyramidal inclusion in gallium arsenide (001): distribution of $\overline{E}_2$ (a) on the vertical plane VPQ and (b) on the horizontal plane through the centroid G of Fig. 10.

validated by comparison with analytical solutions. Numerical simulations have been presented for a pyramidal QD in the substrates of gallium arsenide (GaAs) (001).

References

Andreev, A.D., Downes, J.R., Faux, D.A., O'Reilly, E.P., 1999. Strain distribution in quantum dots of arbitrary shape. J. Appl. Phys. 86, 297–305.

Benabbas, T., Francois, P., Androussi, Y., Lefebvre, A., 1996. Stress relaxation in highly strained InAs/GaAs structures as studied by finite element anlaysis and transmission electron microscopy. J. Appl. Phys. 80, 2763–2767.

Chu, H.J., Wang, J., 2005. Strain distribution in arbitrarily shaped quantum dots with nonuniform composition. J. Appl. Phys. 98, 034315.1–034315.7.

Constantin, C., Martinet, E., Leifer, K., Rudra, A., Lelarge, F., Kapon, E., Gayral, B., Gerard, J.M., 2000. Strained V-groove quantum wires in multidimensional microcavities. Mater. Sci. Eng. B 74, 158–164.

Davies, J.H., 1998. Elastic and piezoelectric fields around a buried quantum dot: a simple picture. J. Appl. Phys. 84, 1358–1365.

Deeg, W.F., 1980. The analysis of dislocation, crack and inclusion problems in piezoelectric solids. PhD thesis, Stanford University.
Dunn, M.L., 1994. Electroelastic Green's functions for transversely isotropic piezoelectric media and their application to the solution of inclusion and inhomogeneity problems. Int. J. Eng. Sci. 32, 119–131.
Eshelby, J.D., 1957. The determination of the elastic field of an ellipsoidal inclusion, and related problems. Proc. R. Soc. Lond. A 241, 376–396.
Eshelby, J.D., 1961. Elastic inclusions and inhomogeneities. In: Sneddon, I.N., Hill, R. (Eds.), Progress in Solid Mechanics, vol. 2. North-Holland, Amsterdam, pp. 89–140.
Faux, D.A., Pearson, G.S., 2000. Green's tensors for anisotropic elasticity: application to quantum dots. Phys. Rev. B. 62, R4798–R4801.
Fu, Y., Zhao, Q.X., Ferdos, F., Sadeghi, M., Wang, S.M., Larsson, A., 2001. Strain and optical transition in InAs quantum dots on (0 0 1) GaAs. Superlattices Microstruct. 30, 205–213.
Gel'fand, I.M., Graev, M.I., Vilenkin, N.Y., 1966. Generalized Functions, vol. 5. Academic Press, New York.
Grundmann, M., Stier, O., Bimberg, D., 1994. Symmetry breaking in pseudomorphic V-groove quantum wires. Phys. Rev. B 50, 14187–14192.
Grundmann, M., Stier, O., Bimberg, D., 1995. InAs/GaAs pyramidal quantum dots: Strain distribution, optical phonons, and electronic structure. Phys. Rev. B 52, 11969–11981.
Holy, V., Springholz, G., Pinczolits, M., Bauer, G., 1999. Strain induced vertical and lateral correlations in quantum dot superlattices. Phys. Rev. Lett. 83, 356–359.
Jogai, B., Albrecht, J.D., Pan, E., 2003. The effect of electromechanical coupling on the strain in AlGaN/GaN heterojunction field effect transistors. J. Appl. Phys. 94, 3984–3989.
Johnson, H.T., Freund, L.B., 2001. The influence of strain on confined electronic states in semiconductor quantum structures. Int. J. Solids Struct. 38, 1045–1062.
Kikuchi, Y., Sugii, H., Shintani, K., 2001. Strain profiles in pyramidal quantum dots by means of atomistic simulation. J. Appl. Phys. 89, 1191–1196.
Kret, S., Benabbas, T., Delamarre, C., Androussi, Y., Dubon, A., Laval, J.Y., Lefebvre, A., 1999. High resolution electron microscope analysis of lattice distortions and in segregation in highly strained In0.35Ga0.65As coherent islands grown on GaAs (0 0 1). J. Appl. Phys. 86, 1988–1993.
Lelarge, F., Constantin, C., Leifer, K., Condo, A., Lakovlev, V., Martinet, E., Rudra, A., Kapon, E., 1999. Effect of indium segregation on optical properties of V-groove InGaAs/GaAs strained quantum wires. Appl. Phys. Lett. 75, 3300–3302.
Lin, G., 2001. Studies on semiconductor quantum structure lasers. PhD thesis, National Chiao Tung University, Taiwan.
Martinet, E., Dupertuis, M.A., Reinhardt, F., Biasiol, G., Kapon, E., Stier, O., Grundmann, M., Bimberg, D., 2000. Separation of strain and quantum-confinement effects in the optical spectra of quantum wires. Phys. Rev. B 61, 4488–4491.
Medeiros-Ribeiro, G., 2002. Epitaxial growth of strained nanocrystals. Phys. Stat. Sol. 230, 443–450.
Mura, T., 1987. Micromechanics of Defects in Solids, second ed. Martinus Nijhoff, Dordrecht.
Notomi, M., Hammersberg, J., Weman, H., Nojima, S., Sugiura, H., Okamoto, M., Tamamura, T., Potemski, M., 1995. Dimensionality effects on strain and quantum confinement in lattice-mismatched InAsxP1 − x/InP quantum wires. Phys. Rev. B 52, 11147–11158.
Pan, E., 2002a. Elastic and piezoelectric fields around a quantum dot: Fully coupled or semi-coupled model. J. Appl. Phys. 91, 3785–3796.
Pan, E., 2002b. Elastic and piezoelectric fields in substrates GaAs (0 0 1) and GaAs (1 1 1) due to a buried quantum dot. J. Appl. Phys. 91, 6379–6387.
Pan, E., Yang, B., 2001. Elastostatic fields in an anisotropic substrate due to a buried quantum dot. J. Appl. Phys. 90, 6190–6196.
Pan, E., Yang, B., 2003. Elastic and piezoelectric fields in a substrate AlN due to a buried quantum dot. J. Appl. Phys. 93, 2435–2439.
Pearson, G.S., Faux, D.A., 2000. Analytical solutions for strain in pyramidal quantum dots. J. Appl. Phys. 88, 730–736.
Pryor, C., Kim, J., Wang, L.W., Williamson, A.J., Zunger, A., 1998. Comparison of two methods for describing the strain profiles in quantum dots. J. Appl. Phys. 83, 2548–2554.
Romanov, A.E., Beltz, G.E., Fischer, W.T., Petroff, P.M., Speck, J.S., 2001. Elastic fields of quantum dots in subsurface layers. J. Appl. Phys. 89, 4523–4531.
Shim, H.W., Choi, R.J., Jeong, S.M., Vinh, L.V., Hong, C.H., Suh, E.K., Lee, H.J., Kim, Y.W., Hwang, Y.G., 2002. Influence of the quantum-well shape on the light emission characteristics of InGaN/GaN quantum-well structures and light-emitting diodes. Appl. Phys. Lett. 81, 3552–3554.
Wang, C.-Y., 1996a. General formalism for piezoelectric crystals of general anisotropy. Appl. Math. Lett. 9 (4), 1–7.
Wang, C.-Y., 1996b. Stress fields produced by dislocations in anisotropic solids. J. Mech. Phys. Solids 44 (3), 293–305.
Wang, C.-Y., Achenbach, J.D., 1995. Three-dimensional time-harmonic elastodynamic Green's functions for anisotropic solids. Proc. R. Soc. Lond. A 449, 441–458.
Yang, B., Pan, E., 2003. Elastic fields of quantum dots in multilayered semiconductors: a novel Green's function approach. J. Appl. Mech. 70, 161–168.
Zhang, X., Sharma, P., 2005. Size dependency of strain in arbitrary shaped, anisotropic embedded quantum dots due to nonlocal dispersive effects. Phys. Rev. B 72, 195345.1–195345.16.